A rapid flood inundation model for hazard mapping based on least squares support vector machine regression

María Bermúdez[1]*, Luis Cea[1], and Jerónimo Puertas[1]

1 Water and Environmental Engineering Group, Departamento de Ingeniería Civil, Universidade da Coruña, A Coruna, Spain

* Corresponding author. Email: mbermudez@udc.es

ABSTRACT

Two-dimensional shallow water models are widely used tools for flood inundation mapping. However, even if High Performance Computing techniques have greatly decreased the computational time needed to run a 2D inundation model, this approach remains unsuitable for applications that require results in a very short time or a large number of model runs. In this paper we test a non-parametric regression model based on least squares support vector machines as a computationally efficient surrogate of the 2D shallow water equations for flood inundation mapping. The methodology is initially applied to a synthetic case study consisting of a straight river reach flowing towards the sea. A coastal urban area is then used as a real test case. Discharge in three streams and tide levels are used as predictor variables to estimate the spatial distribution of maximum water depth and velocity in the study area. The suitability of this regression model for the spatial prediction of flood hazard is evaluated. The results show the potential of the proposed regression technique for fast and accurate computation of flood extent and hazard maps.

Keywords: flood hazard, flood inundation, Iber model, shallow water equations, support vector machine

This article has been accepted for publication and undergone full peer review but has not been through the copyediting, typesetting, pagination and proofreading process, which may lead to differences between this version and the Version of Record. Please cite this article as doi: 10.1111/jfr3.12522

1. INTRODUCTION

Physically-based flood inundation models are widely used tools for simulating river hydraulics and floodplain inundation processes. In these models, the flood propagation is generally described by the two-dimensional shallow water equations (2D-SWE), which must be solved using an appropriate numerical technique. Models solve either the full or simplified forms of these equations, as the local inertial approximation or the diffusive wave approximation (Neal et al. 2012). In practice, an inevitable compromise between accuracy and efficiency must be found when defining the spatial resolution of the numerical mesh and the time discretization (Chen et al. 2012). Higher accuracy can be obtained by increasing the physical complexity and the spatial and temporal resolution of a model, but at the cost of higher computation time.

This conventional physically-based approach is hence generally impractical for applications that require results in a very short time or a large number of model runs. A typical example is a probabilistic analysis such as the propagation of uncertainty in a Monte Carlo context, which involves the evaluation of thousands model runs. A few Monte Carlo probabilistic analyses using 2D-SWE models have been presented in the literature but the number of runs is generally limited to a few hundreds (Cea et al. 2011; Fraga et al. 2016), which limits the number of parameters that can be analyzed and the statistical significance of the results. Real-time forecasting systems are another example where fast computation is imperative to issue flood warnings with sufficient lead-time. In these kinds of applications, a possible way to reduce significantly the computation time is the development of computationally more efficient surrogates of these models. A first approach is to develop simplified physically-based models that contain less detail than the original model (Razavi et al. 2012). In the context of urban flood modelling, this typically involves the use of coarser grids and the development of sub-grid models to account for topographic variability that is too small to be resolved with the computational mesh (Cea & Vázquez-Cendón 2009; Guinot 2012; Schubert & Sanders 2012; Chen et al. 2012; Bruwier et al. 2017). The use of nested grids has also been proposed in some studies that require a large computational domain (Bermúdez et al. 2017; Comer et al. 2017). Nested grids provide very high spatial resolution in selected areas of interest without incurring into the computational expense of fine grid resolution over the entire model domain. Model complexity can also be reduced by solving simplified forms of the 2D shallow water equations (Neal et al. 2012). Other works have adopted a cellular automata approach to minimize the need for solving complex and computationally expensive equations (Ghimire et al. 2013; Liu et al. 2015; Guidolin et al. 2016). Instead of solving the full or simplified forms of the 2D-SWE, local state transition rules are used to determine the flow movement from one cell to another.

For many applications, a simplified physically-based surrogate might yield insufficient computational improvement. Besides, the main concern in many practical situations is making accurate and timely flood predictions, with limited interest in the physical processes represented in the original model. In these cases, data driven models that emulate the original model responses can constitute an alternative approach (Razavi et al. 2012; Solomatine & Ostfeld 2008). Data driven models empirically approximate the response of an original simulation model for various values of the explanatory variables. Popular function approximation techniques used as response surrogates in the water resources field are conventional regression methods, either linear or non-linear, and artificial intelligence (AI) based methods such as least-squares support vector machines (LS-SVM) or artificial neural networks (ANN). These latter models are becoming increasingly popular in water resources modelling due to their capability of emulating complex relationships.

AI-based models have been widely applied for rainfall-runoff modelling and streamflow (or stage) forecasting (Yaseen et al. 2015). Some applications to flood inundation modelling have also been investigated, although these are scarce. Chang et al. (2010) employed linear regression models and ANNs to build a regional flood inundation forecasting model, which provided flood inundation maps that compared well with those obtained with a 2-D non-inertial overland flow model. ANNs have also been successfully used to identify flooding and

estimate flood volumes in the context of urban pluvial simulations (Bermúdez et al. 2018). Liu & Pender (2015) investigated the use of LS-SVM regression to predict the evolution of water depth and velocity obtained from a fine grid SWE model at given locations, achieving good predictive results. In the works of in et al. (2013) and Jhong et al. (2017), LS-SVM is used to yield inundation depth forecasts at control points, which are then translated into a spatial forecast based on geographic information. All the aforementioned studies have shown that, once conveniently calibrated, these computationally less demanding approaches can result in comparable predictions to physically-based models. Compared to other machine learning methods, LS-SVMs have demonstrated a high accuracy and efficiency, which means that they can be more rapidly trained with real-time data and are more suitable to be integrated with disaster warning systems (Lin et al. 2013; Jhong et al. 2017).

In this paper we further elaborate on the suitability of AI-based techniques for flood simulation. We test a non-parametric regression model based on least squares support vector machines (LS-SVM model) as a computationally efficient surrogate of a 2D-SWE model for flood inundation mapping. Unlike the previous works mentioned above, this paper is focused on the prediction of maximum water depth and velocity, with the aim of deriving flood hazard maps. The methodology is initially applied to a simplified synthetic case study that consists of a straight river reach flowing into the sea. The simplified case is used to analyse the capability of the LS-SVM model to reproduce the maximum values of the water depth given by a 2D-SWE model during a flood event, as well as the evolution in time of the water depth (stage hydrographs). We then extend the methodology to a real case study. A coastal urban area of approximately 2 km^2 is used for this purpose. In this case, maximum values of flood depth and velocity at approximately 25,000 control points are used to produce flood hazard maps.

In both cases the software Iber (Bladé et al. 2014) is used to solve the 2D-SWE and to generate the calibration and validation datasets for the LS-SVM model. The predictor variables are the flood hydrographs and the tide level at the model outlet. The predictands are the water depth and velocity at a number of control points. The predictive accuracy and computational efficiency of the LS-SVM model are evaluated in both cases by comparing the predictands obtained with the LS-SVM model to those obtained with the 2D-SWE model.

2. METHODOLOGY

2.1. Two-dimensional shallow water models

The shallow water model used in this work is the software Iber (Bladé et al. 2014). This model solves the 2D depth-averaged shallow water equations in order to compute the spatial and temporal evolution of the water depth and the two horizontal components of the depth-averaged velocity. The model has been validated in previous studies and publications, showing its capabilities to represent 2D free surface shallow flows and river inundation processes(Cea & French 2012; Cea & Bladé 2015; Bladé et al. 2014; Fraga et al. 2016). For a detailed description of the model the reader is referred to (Bladé et al. 2014) and the references therein.

Bed friction is evaluated using the Manning's formula, the Manning’s roughness coefficient being the only parameter of the model. Small-scale topographic variations are explicitly represented in the model, instead of parameterizing their effects via subgrid scale models or artificial roughness (Bermúdez & Zischg 2018).

This physics-based model is assumed to provide the best representation of the system behavior for the purposes of this work, the simulation results being applied as synthetic data to calibrate and validate the surrogate model. The use of simulation data instead of field measurements is a common approach when developing surrogate models (Kroll et al. 2017), due to the need for enough training data to achieve appropriate generalization. The main advantage is that simulations can yield spatially and temporally detailed

data for a comprehensive set of flood events. However, if enough monitoring data were available, the surrogate model could be trained directly to this data.

2.2. LS-SVM regression models

LS-SVM is a non-parametric regression technique that relates a dependent variable (predictand) with a set of explanatory variables (predictors). LS-SVM has been derived from the original support vector machine model (Vapnik 1998), a kernel-based learning method for linear and non-linear classification problems. The mathematical theory behind the LS-SVM method is well established and can be found in (Suykens et al. 2002). A detailed mathematical description of the method is not given here for the sake of conciseness.

In the applications presented in this paper, the dependent variables are the water depth (h) and velocity (v) computed by a 2D-SWE model at a specific location on the study area. For a given study area and model setup, the water depth and velocity predicted by a 2D-SWE model depends only on the boundary conditions, which are typically the water discharge (Q) at the upstream boundary and the water level (Zs) at the downstream boundary. Thus, the LS-SVM model is intended to establish a relation between the values of Q and Zs imposed as boundary conditions in the 2D-SWE model, and the water depth and velocity (h,v) at a specific location.

The LS-SVM needs to be calibrated with a set of predictors and predictands. In our case those are obtained by running the 2D-SWE model in a number of calibration cases. Once calibrated, the LS-SVM model will predict the value of h and v for any given pair of Q and Zs. Notice that this relation is valid for a specific location and thus, a different LS-SVM regression must be calibrated for each spatial point. In order to validate its performance, we run the 2D-SWE model in a number of validation cases and compare its results with the values of h and v predicted by the LS-SVM model.

In this work the LS-SVM models were developed using Matlab software (version 2011a) and the toolbox StatLSSVM (Brabanter et al. 2013).

2.3. Synthetic case study

2.3.1. Case description

The methodology is first validated in the context of a simplified synthetic case study of an idealized valley topography. We consider a 1 km long straight river reach flowing towards the sea, with a longitudinal slope of 0.001. The cross section has a 2.5 m depth trapezoidal channel and two symmetric floodplains (Figure 1). Four control points located along the main channel are used to evaluate the performance of the regression models (Figure 2). The models are built to predict the maximum flood depths and to reproduce the time evolution of the water depth during flood events.

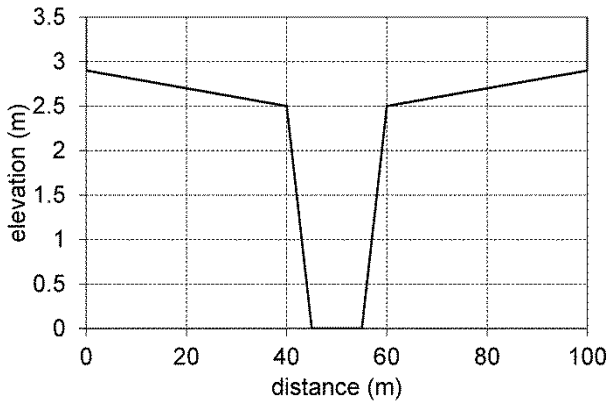

Figure 1. River cross section of the synthetic case study.

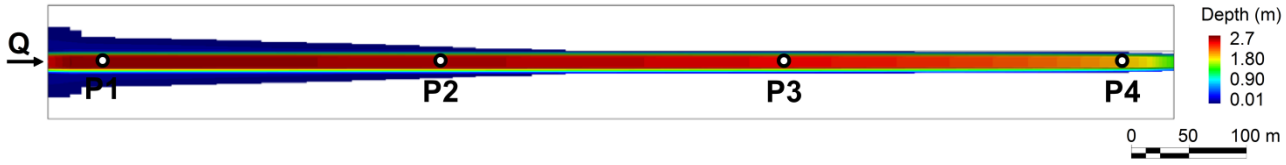

Figure 2. Example of water depth map predicted by the 2D-SWE in the synthetic case study. Location of control points (P1-P4).

2.3.2. Generation of the dataset for the regression models

The dataset for the LS-SVM model was generated with a 2D-SWE model of the synthetic case. The domain was discretized with a structured mesh of 10,200 quadrilateral elements. A Manning roughness coefficient of 0.032 $s \cdot m^{-1/3}$ was selected to compute bed friction. The hydrograph of the river (Q in Figure 2) and the sea surface elevation were imposed at the upstream and downstream boundaries.

In order to generate the calibration and validation datasets for the LS-SVM model, 200 simulations were run with the 2D-SWE model. Each model run is defined by a discharge time series (the upstream hydrograph) and a constant water elevation (the downstream sea level). The hydrograph has a triangular shape defined by the peak discharge, the time to peak and the duration of the recession limb. For each simulation a different combination of these variables was used to define the upstream hydrograph. The peak discharge was varied from 60 to 120 m^3/s, the time to peak from 600 to 6000 s and the recession limb time from 1000 to 10000 s. A constant water elevation at the reach outlet varying from 0.5 m to 2.5 m was defined for each run. Runs with duration in the order of 250 minutes were calculated, resulting in a computation time of 5 minutes on standard desktop computing hardware.

For each model run, the time series of water depth obtained with the 2D-SWE at the 4 control points shown in Figure 2 were extracted and used as predictands. Two different LS-SVM regression models (which will be referred to as model A and model B) were developed, which differ on the dependent and predictor variables used. In the regression model A, the maximum depth obtained with the 2D-SWE model at each control point constitutes the predictand variable. The predictor variables in this model are the peak discharge of the inlet hydrograph and the water level prescribed at the channel outlet. In the regression model B, the predictand is the instantaneous water depth at each control points at any time during the flood event (not necessarily the maximum depth value during the event). The predictor variable is comprised of the current and 5-min antecedent discharge value and the water level at the channel outlet. Regression model A is thus intended to be applied to predict only the maximum water depth at each control point during the flood event, whereas regression model B is set up to predict the time evolution of the water depth at each control point.

In order to split the input dataset into validation and calibration runs, the Maximum Dissimilarity Algorithm (MDA) was used (Kennard & Stone 1969). The aim of MDA is to select a subset of a database that represents the diversity of the data. This is done by maximizing the dissimilarity between the vectors in the subset. In this work the MaxMin version of the algorithm was used (Willett 1996). The algorithm developed by (Polinsky et al. 1996) was used to calculate the dissimilarity between a vector and a subset. The 200 model runs were divided into 50 calibration runs and 150 validation runs, based on the peak discharge and water level pairs that define each run. Given the limited number of control points considered in this synthetic test case, the calibration process takes only of the order of a few seconds on standard desktop computing hardware, and the calculation time of the calibrated model requires less than a second.

2.4. Real case study

2.4.1 Case description

In a second step, the methodology is validated in the real case study of the urban area of Vilagarcia de Arousa (Northwest of Spain). It is a coastal town recurrently affected by flooding, which is classified as a high potential flood risk area by the regional authorities. It lies at the mouth of the river Con, which flows into the sea in the Ria de Arousa estuary. The basin of the river Con has a total area of 24 km^2 and its topography is relatively steep, the maximum height being 640 m.a.s.l. It is divided into three sub-catchments, the main one corresponding to the river Con and extending over the central and northern part of the catchment (Q_1 outlet in Figure 3, with an area of 16.3 km^2). The low concentration time of the basin, as well as the tide level play a role in the flooding of the urban area. The regression models are built to predict maximum flood depth and velocities in this area, and subsequently derive flood hazard maps.

2.4.2. Generation of the dataset for the regression models

A shallow water model of the urban area of Vilagarcía de Arousa was set up using the software Iber. The domain was discretized into an unstructured computational mesh of 111630 triangular elements, with element sizes ranging from 1 to 10 m. The topography was defined from a 1 m resolution gridded LIDAR-based digital surface model. The resulting DEM was enhanced by integrating the bathymetry of the main water streams and the geometry of structures and buildings, the latter being represented as void areas. Thus, the model incorporates the topographic complexity of the urban area and represents flows at the scale of individual buildings. Bed friction was computed with Manning's formula. Given the accurate representation of the topography and man-made structures in the model, the roughness coefficient is set to represent only small scale roughness, and typical values can be expected to give a good prediction of inundated areas (Horritt & Bates 2002). In this case, the following values were selected for the Manning roughness coefficient: 0.025 $s \cdot m^{-1/3}$ for the river bed, 0.032 $s \cdot m^{-1/3}$ for urban vegetated areas and 0.020 $s \cdot m^{-1/3}$ for concrete surfaces. At the upstream open boundaries, the hydrographs of the three main watercourses of the basin were imposed (Q1, Q2 and Q3 in Figure 3). At the downstream sea boundary, the water surface elevation time series was fixed in order to reproduce the tide level variation.

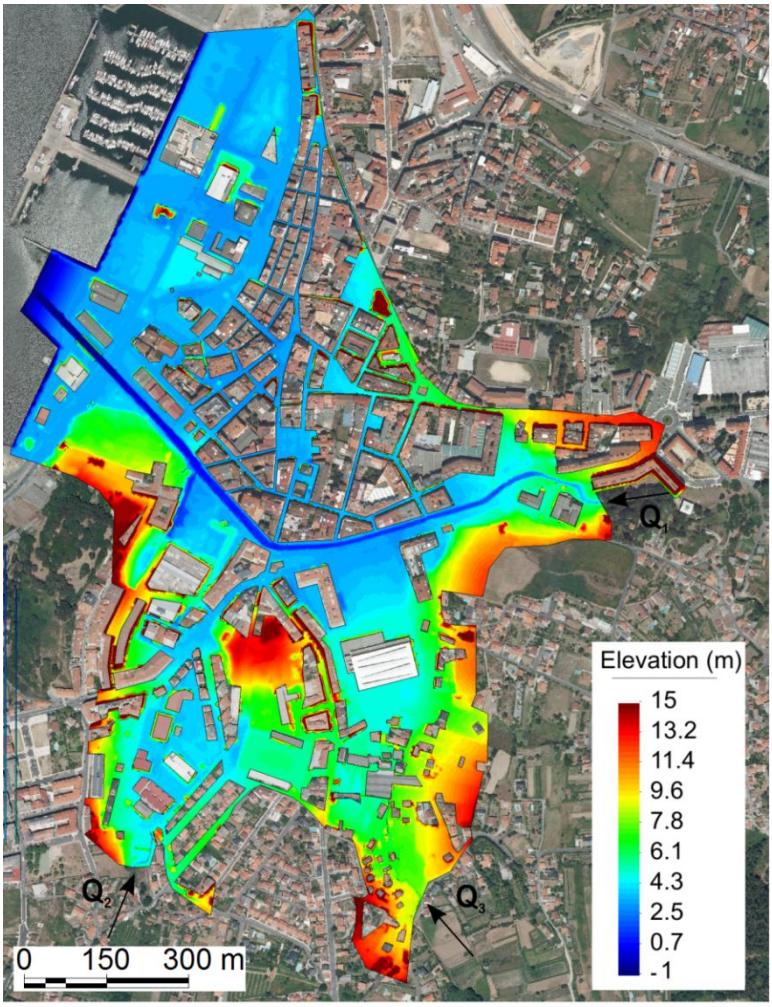

Figure 3. Topography used in the 2D-SWE model overlaid onto an aerial image of the study area. The arrows represent the upstream boundary conditions, which correspond to the three main watercourses of the basin.

In order to generate the calibration and validation datasets for the LS-SVM model, 100 simulations were run with the 2D-SWE model. Each model run is defined by three discharge time series (the upstream hydrographs) and a water elevation time series (the tide). Since the catchment is scarcely gauged, a distributed hydrological model of the river Con catchment driven by rainfall data was used to provide feasible input data for the hydraulic model (Figure 4). The 15 historical rainfall events with higher daily rainfall amounts during the period 2000-2015, recorded in a meteorological station of the Regional Weather Forecast Agency (MeteoGalicia) located in the catchment, were used. Initial abstraction and potential infiltration values in the range of 0-20 mm and 0-5 mm/h, respectively, were considered in the hydrological simulation. In this way, the upstream hydrographs used in the 2D-SWE model are produced using an ensemble of distributed hydrologic model simulations driven by measured precipitation data and perturbed parameter sets. Unlike in previous works in which a certain shape of the inflow hydrograph is assumed (Liu & Pender 2015), the generated hydrographs vary in both shape and volume. Peak flows range from 1 to 106 m^3/s for Q1, from 0.3 to 24 m^3/s for Q2, and from 0.5 to 22 m^3/s for Q3 (Figure 4). In all cases a very low river discharge equal to mean annual discharge was considered as initial discharge. Given that the same initial conditions were used in all the simulations, it is not possible to explore its influence on the predicted maximum inundation height and velocity. At the sea boundary, four different water surface elevation time series were defined, corresponding to spring tide or neap tide (3 m vs. 1.8 m tide range) and starting either in ebb tide or rising tide (6 hours offset). Every simulation was run for 24 hours, resulting in a computation time of 14 h on standard desktop computing hardware.

For each model run, the maximum flood depth (h) or velocity (v) obtained with the 2D-SWE model constitutes the dependent variable of the regression models. Raster maps of these variables with a spatial resolution of 1 m were extracted for each model run. The predictor (or independent) variables were derived from the discharge and tide data time series prescribed at the boundaries of the numerical model. Different types of input vectors were considered to develop the regression models and their performance was assessed in (Cea et al. 2016). Following this previous analysis, a combination of four parameters was selected. For each of the three hydrographs, the maximum discharge rate exceeded during a time period of 1 hour was selected as the predictor variable (Q1max, Q2max and Q3max). In the case of the tide level time series, the maximum water level for each event was considered (Zsmax). These variables were normalized between [0,1] with a simple linear transformation. Over 25,000 points evenly distributed in the study area were selected and a non-parametric regression model based on LS-SVM (Suykens et al. 2002) was calibrated at each point. As in the previous test case, the Maximum Dissimilarity Algorithm (MDA) was used to split the input dataset into validation and calibration runs.

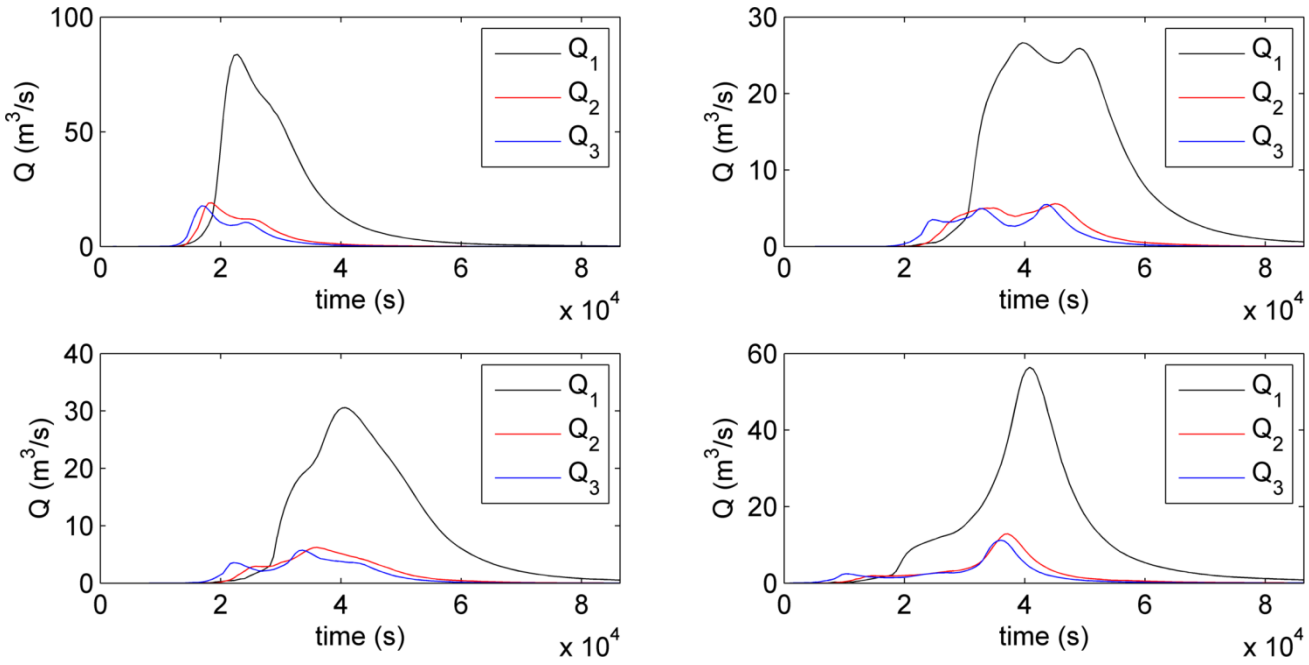

Figure 4. Example of inflow hydrographs prescribed at the upstream open boundaries of the 2D-SWE model. The location of the three open boundaries (Q1, Q2 and Q3) is indicated in Figure 3.

3. RESULTS AND DISCUSSION

3.1. Synthetic case study

A comparison between the water depths computed by the 2D-SWE model and the regression models A and B is shown in Figure 5. Regression model A uses the peak discharge of the inflow hydrograph and the downstream water level as independent variables. This model can accurately predict the peak flood depths during the simulation at all the control points (Figure 5a). The global mean absolute error considering all runs and control points is below 3 cm.

However, the capability of model A to reproduce the evolution of water depth during the flood event is much worse (Figure 5b). This is because regression model A is trained only with the peak discharge data. This indicates that it is necessary to include additional predictor variables in the regression model in order to simulate the time evolution of the water depth during the flood event accurately. Regression model B uses both current and 5-min antecedent discharge as predictor data, in addition to the downstream water level. The

time evolution of the water depth is accurately predicted with model B (Figure 5c). The global mean absolute error considering all points is below 1 cm in this case.

The above results are further illustrated in Figure 6, which shows the water depth evolution computed by the 2D-SWE and the LS-SVM models in two typical runs. The maximum water depth during the event is accurately predicted by the two LS-SVM models. However, the regression model A gives a significant discrepancy in the timing and shape of the depth hydrographs, while the model B captures much better the time evolution of the water depth.

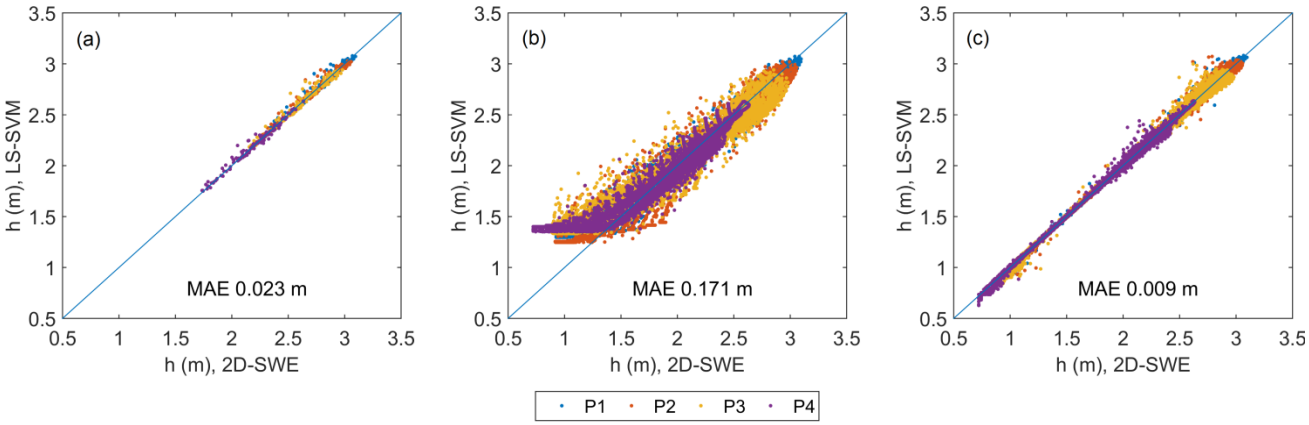

Figure 5. Scatter plots of water depths computed with the 2D-SWE and the LS-SVM models in validation, considering: (a) Regression model A applied to predict peak depths only; (b) Regression model A applied to predict 5-min resolution water depths; (c) Regression model B applied to predict 5-min resolution water depths. Note: MAE is the global mean absolute error on the 4 points and for the ensemble of validation runs.

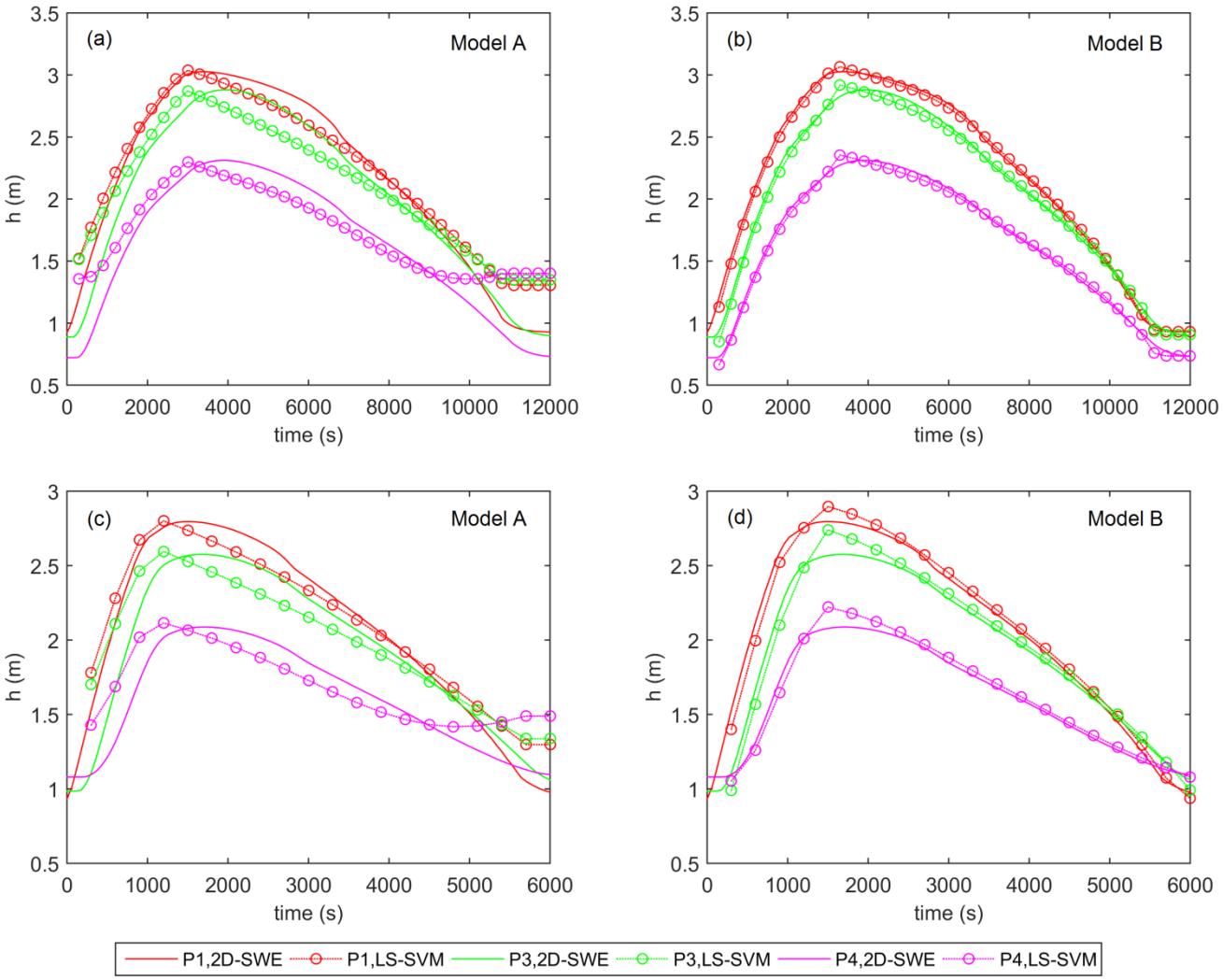

Figure 6. Water depth time series at control points P1, P3 and P4 computed with the 2D-SWE model and with the LS-SVM models in two illustrative simulations: (a) Simulation 1, regression model A; (b) Simulation 1, regression model B; (c) Simulation 2, regression model A; (d) Simulation 2, regression model B.

These results suggest that, if there is only interest in the maximum water depths achieved during an event (as it is often the case in flood hazard mapping), it suffices to use the peak discharge and downstream water level as predictor variables for obtaining accurate estimates of peak depths. On the other hand, in order to represent properly the flood dynamics during the whole event it is necessary to use a model calibrated with stage and discharge hydrographs and not only with peak values.

3.2. Real case study

3.2.1. Number of calibration runs

In order to analyse the influence on the regression accuracy of the number of calibration runs (k), several tests were performed changing k from 5 to 50. The remaining runs were used to validate the calibrated LS-SVM model. The overall performance of the LS-SVM model was evaluated by calculating the global mean absolute error at the circa 25,000 control points in the study area (MAE_{global}), in calibration and in validation.

In calibration, the global mean absolute error of the depth and velocity predictions shows little variation with the number of calibration runs, being in the order of 0.015 m and 0.020 m/s, respectively (Figure 7). In

validation, the error increases as the number of calibration runs decreases, ranging from 0.016 m (k=50) up to 0.053 m (k=5) and from 0.019 m/s (k=50) up to 0.050 m/s (k=5) for the depth and velocity predictions. However, the errors remain practically constant in the interval k=40-50, so no significant improvement is achieved if the number of calibration runs is above 40 (Figure 7). Therefore, the LS-SVM model was calibrated with the data of 40 flood events and validated using the remaining 60 flood events.

The calibration process takes about 1 hour on standard desktop computing hardware. The calculation time of the calibrated model is much shorter, in the order of a few seconds.

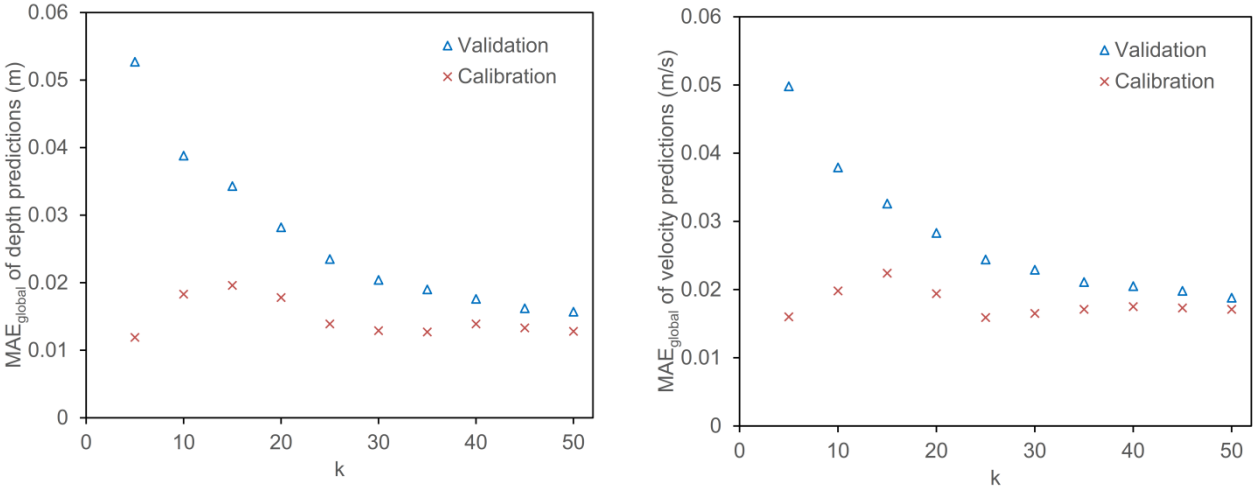

Figure 7. Global mean absolute error of the depth predictions (left) and the velocity predictions (right) in calibration and validation as a function of the number of calibration runs (k).

3.2.2. Model performance

Prior to using the point predictions of the LS-SVM model to derive spatial maps of water depth, velocity and flood hazard, it is important to evaluate the performance of the LS-SVM regression model. The predictions at all control points for the validation runs are shown in Figure 8 as two-dimensional histograms (binned scatter plots) that compare the water depths and velocities estimated with the LS-SVM model with those computed with the 2D-SWE model. In the case of depth predictions, the points are evenly distributed around the 1:1 line and the scatter is fairly uniform for the whole range of depths. The LS-SVM model slightly overestimates the higher depth values (h> 3m) (Figure 8b), but the scatter of the data is fairly symmetrical for water depths lower than 2.5 m, with about the same number of data points above and below the 1:1 line. In the case of velocity predictions, the scatter is larger at the higher range of velocities (v>3m/s), but no obvious underestimation or overestimation occurs. All the points are scattered more or less symmetrically about the 1:1 line.

The performance of the LS-SVM model at each control point was quantified using the pointwise mean absolute error (MAE) computed for each control point from the ensemble of validation runs. Figure 9 shows the histograms of predictive error in depth and velocity. The global mean absolute error of the depth and velocity predictions is only 0.018 m and 0.020 m/s respectively, while the 90^{th} percentiles are 0.034 m and 0.05 m/s. These values are much lower than the expected accuracy of 2D physically based models in flood inundation applications, which implies that the LS-SVM can be used as a surrogate model of the 2D-SWE without introducing a relevant source of error in the results.

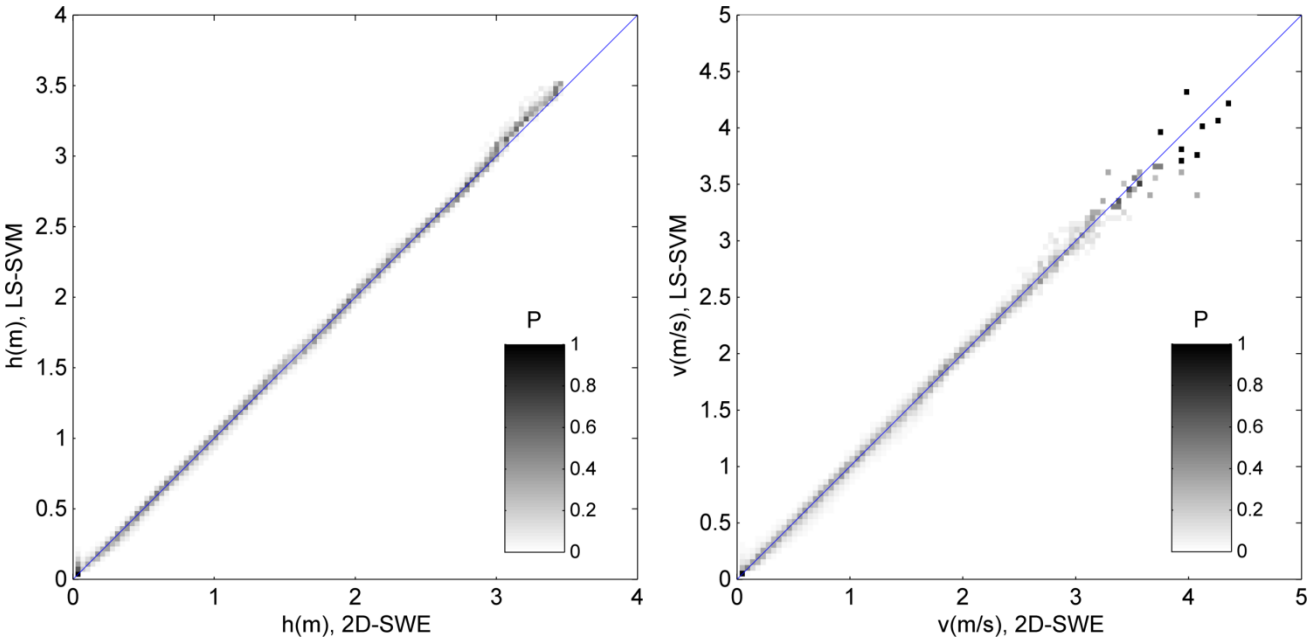

a) Depth b) Velocity

Figure 8. Two-dimensional histogram of the LS-SVM predictions vs. 2D-SWE predictions for the water depth (left) and velocity (right) using 100x100 bins. The color bar shows the relative frequency in the histogram, being the sum of all frequencies in each x-direction bin equal to unity.

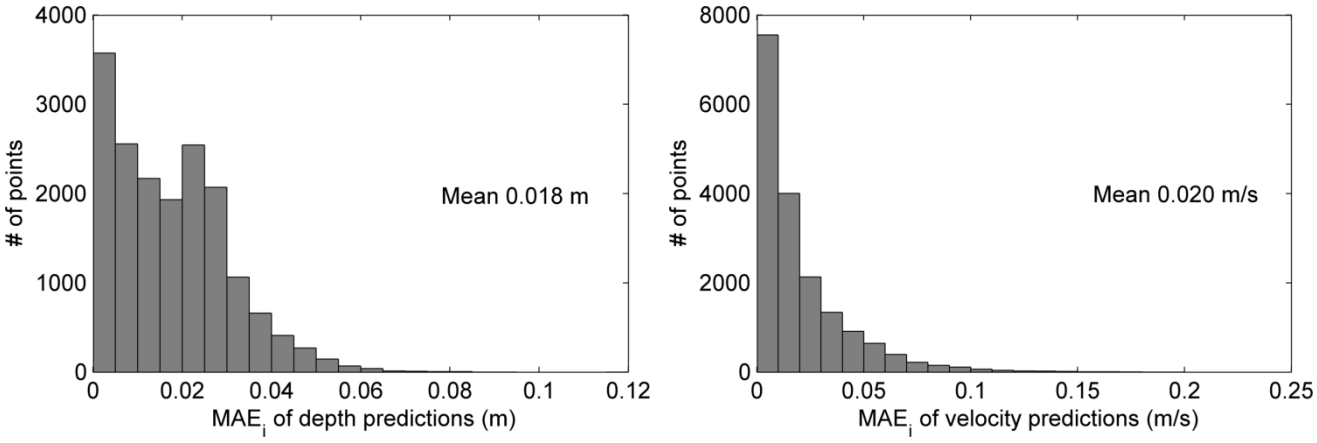

a) Depth b) Velocity

Figure 9. Histogram of mean absolute error of depth and velocity predictions at the different points.

The spatial distribution of the regression MAE (Figure 10) provides information on the local performance of the LS-SVM surrogate. The worst model predictions are not located in a particular region, but scattered throughout the spatial domain. There is some correspondence between the scatter map of the mean absolute errors of depth and velocity (Figures 10a and 10b), i.e., between the points of relative high MAE in depth and MAE in velocity. However, this is not always the case, and an accurate prediction of only one of the two variables is achieved at certain points.

The LS-SVM model is able to emulate diverse non-linear relationships between the predictor and dependent variables, as illustrated in Figures 11 and 12. These relationships cannot be adequately modelled using standard regression techniques (e.g., a multiple linear regression), as demonstrated in (Cea et al. 2016). Close to the sea, at control point P1, the influence of the tide is well captured by the regression model (Figure 11a). At that point, for the lower range of discharges, the maximum depth predictions depend largely on the maximum tide level, and the rating curve bifurcates. The lower branch is associated with the neap tide, with a

maximum tide level of 1.26 m; whereas the upper branch corresponds to the spring tide, with a maximum tide level of 1.81 m. The influence of the tide on the depth predictions decreases as we move upstream along the main channel. Its influence is only perceived along a 600-m reach. At points located further upstream in the main channel (control point P2), the relationship between the upstream discharge and the depth follows a single curve with very little scatter (Figure 11b). At that point, the maximum depth and velocity predictions depend mainly on the maximum discharge of the main watercourse. Flow velocity increases as the discharge increases for inbank flow, and is nearly constant for discharges beyond bankfull stage (Figure 12b). In the upstream regions of the right floodplain (control point P4), the maximum depth is also mainly dependent on the discharge (Figure 11d). The influence of the other two tributaries discharges is limited spatially to the upstream regions of the left floodplain (control point P3), and its effect is reflected in a wider scatter in the discharge-depth relationship (Figure 11c). Given that the same initial upstream discharges (at time=0) were used in all simulations, the effect of different initial conditions on the maximum depth or velocity predictions is not analyzed in this case.

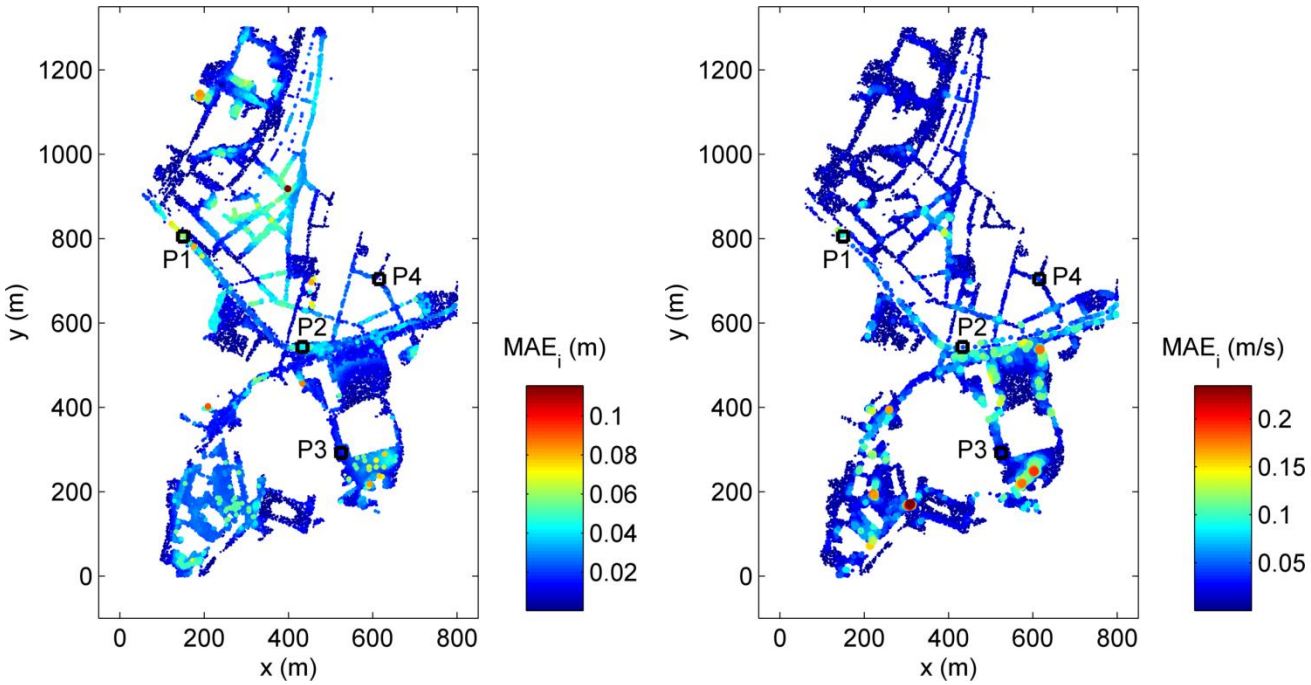

(a) Depth predictions (b) Velocity predictions

Figure 10. Scatter map of the MAE at each point in validation. The size of each marker is proportional to the MAE at that point. The location of the points represented in Figures 7 and 8 is marked by a black square.

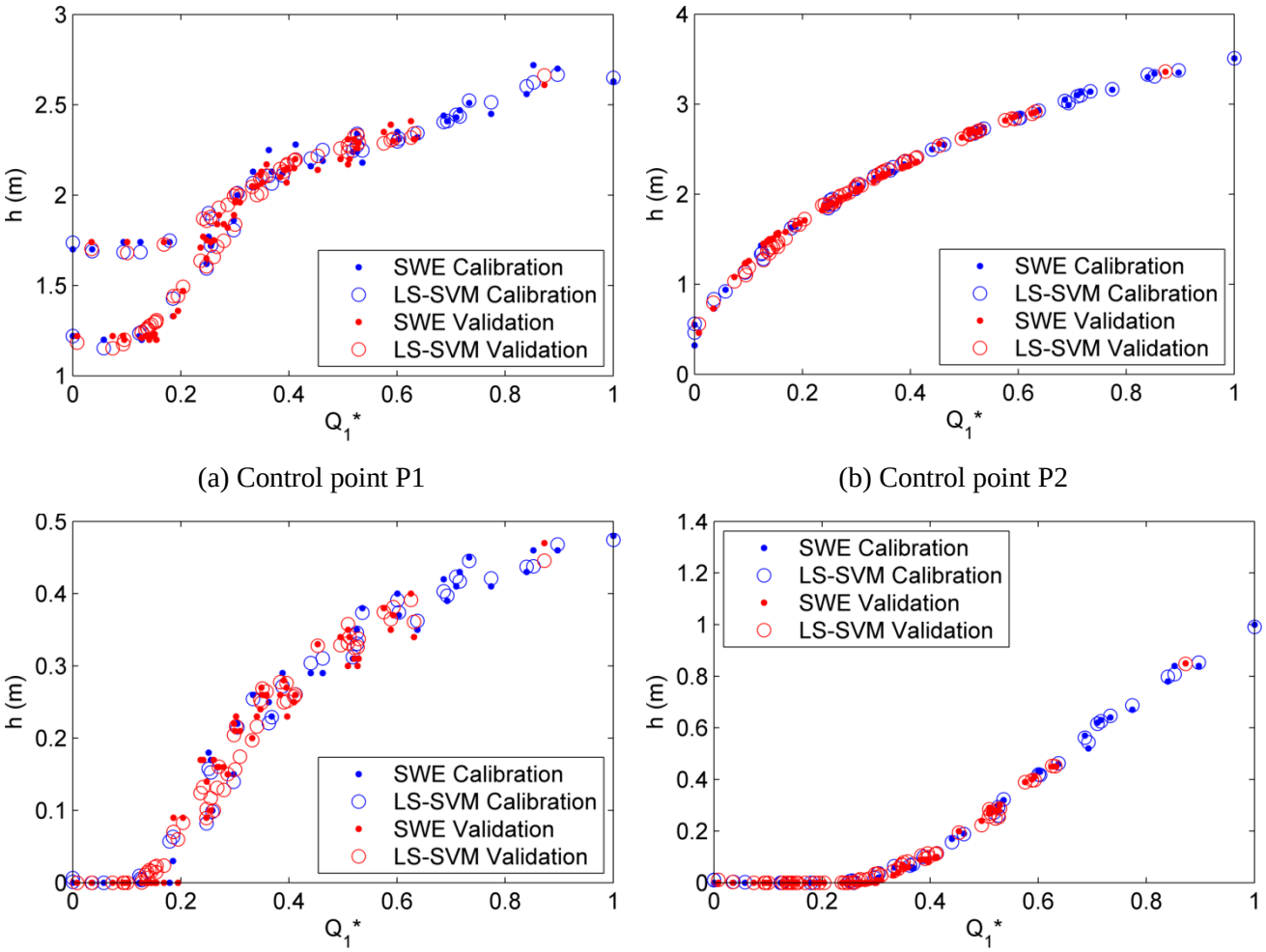

(a) Control point P1

(b) Control point P2

(c) Control point P3

(d) Control point P4

Figure 11. Depth predictions (h) at four representative points (control points P1-P4 in Figure 6) with the 2D-SWE model and the LS-SVM model, as a function of the normalized maximum discharge of the main water course (Q1*).

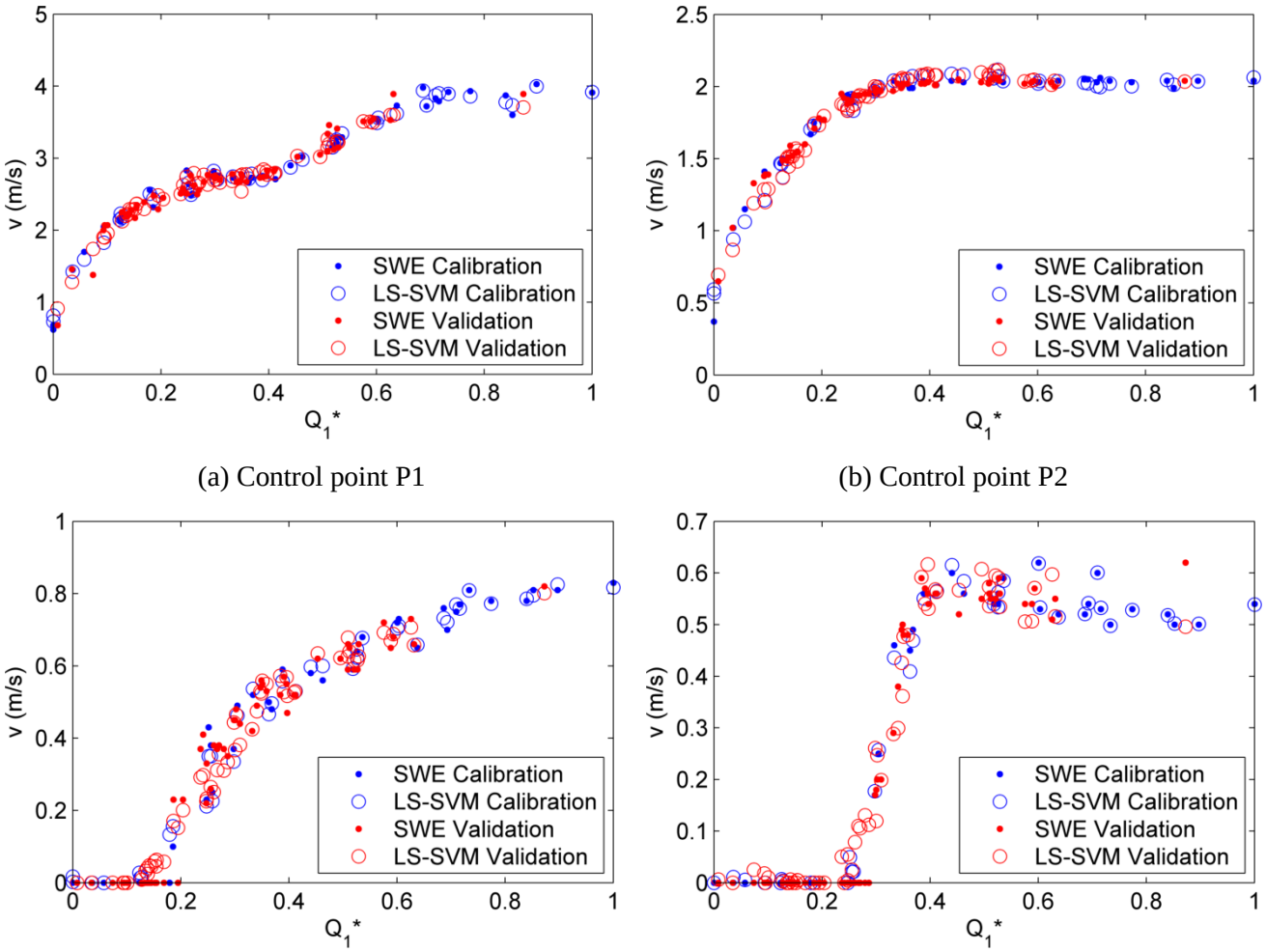

(a) Control point P1

(b) Control point P2

(c) Control point P3

(d) Control point P4

Figure 12. Velocity predictions (v) at four representative points (control points P1-P4 in Figure 6) with the 2D-SWE model and the LS-SVM model, as a function of the normalized maximum discharge of the main water course (Q1*).

3.2.3. Hazard mapping

Hazard mapping gives an estimation of the extent and magnitude of flooding, and it is usually defined as a function of depth and velocity. In this section we derive flood extent and flood hazard maps using the pointwise predictions of depth and velocity obtained with the LS-SVM model. The results are compared with those obtained with the 2D-SWE model in order to evaluate the suitability of the proposed method for flood hazard estimation in real-time forecasting applications.

First, the pointwise predictions of depth and velocity obtained with the LS-SVM model are linearly interpolated into raster maps with the same spatial resolution as the output from the 2D-SWE model (i.e., 1 m) (Figures 13a and 13c). The differences with the corresponding 2D-SWE map are then calculated and visually inspected (Figures 13b and 13d). This visual comparison shows that the interpolation procedure introduces errors in some areas of the map (e.g. in the velocity predictions along the banks of the main river channel), but that LS-SVM depth and velocity maps exhibit a reasonable match with the corresponding 2D-SWE maps. Poor predictions are obtained only in relatively small areas scattered throughout the map.

These maps are subsequently used as a basis for flood extent and hazard zoning. A wet-dry threshold of 0.10 m is considered to delineate flood extent. Flood hazard is determined as a function of water depth and flow velocity, considering six thresholds or categories: 0.20 m, 0.50 m and 1 m for inundation depth; and 0.10 m/s,

0.50 m/s and 1 m/s for flow velocity. Three performance measures are used to quantify how well the LS-SVM model matches the spatial predictions of the 2D-SWE model: precision (p), recall (r) and F1 score, formulated for each flood map as:

$$p=\frac{A}{B}$$
$$r=\frac{A}{C} \qquad (1)$$
$$F1=2\frac{p\cdot r}{p+r}$$

where A is the area correctly predicted in a specific category by the LS-SVM model, B is the total area predicted in that category by the LS-SVM model and C is total area predicted in that category by the 2D-SWE model. A high precision means that most of the area that the LS-SVM model predicts in a certain hazardous category is also predicted in that category by the 2D-SWE model. A high recall means that most of the area predicted by the 2D-SWE model in a certain hazardous category is well captured by the LS-SVM model. The lower and upper bounds of precision and recall are 0 and 1 respectively. In the context of early warning flood forecasting systems, a high recall ensures that the authorities are alerted to take action in most of the actual hazardous areas, whereas a high precision avoids unnecessary actions and preparations in non-hazardous areas. F1 is the harmonic mean of precision and recall, and is equal to 1 when the areas predicted by the LS-SVM and the 2D-SWE model coincide exactly. These metrics are commonly used for evaluating flood inundation models (Aronica et al. 2002; Pappenberger et al. 2007) and their applicability and limitations are further discussed in (Stephens et al. 2014). In the case of flood hazard maps, we employ these metrics to evaluate the binary classification into the different flood intensity categories. Thus, F1 is equal to 1 when the areas classified into a certain flood intensity category by the LS-SVM and the 2D-SWE model coincide exactly.

Table 1 shows the mean performance of the LS-SVM model based on the hazard mapping. The model matches the flood extent well, with high values of recall and precision. Precision is lower than recall, which reflects that the mismatch between the flood extent predicted by the LS-SVM model and the SWE model is mainly related to overestimation. In average, 16% of the surface that the LS-SVM model predicts as flooded is not flooded according to the 2D model, while the LS-SVM model does not capture only 6% of the surface that the 2D model predicts as flooded. The values of the metrics are toward the upper limit of the ones reported in previous studies which have compared numerical model predictions with observed inundation extents (Yu & Lane 2006; Tayefi et al. 2007). This suggests that the errors introduced by the LS-SVM model in the flood extent predictions are acceptable for practical use.

The metrics in Table 1 show that the depth hazard maps predicted by the LS-SVM model are more accurate than the velocity hazard maps. Precision and recall are respectively above 0.87 and 0.92 for all the depth hazard categories, while they diminish to 0.7 for the velocity hazard categories. This suggests that the proposed approach could be used for flood damage assessments relying on depth-damage curves, which are often considered as the main determinant factor to assess urban flood losses (Apel et al. 2009; Kreibich et al. 2009; Tsakiris 2014). On the other hand, it should be applied with caution to high-velocity related hazard criteria, since the performance of the LS-SVM model to capture high velocity regions is slightly worse, as shown in Table 1. The performance of the LS-SVM model is also satisfactory in terms of computational cost. Once the model is calibrated, the simulation time is reduced from 14 hours to a few seconds for each event.

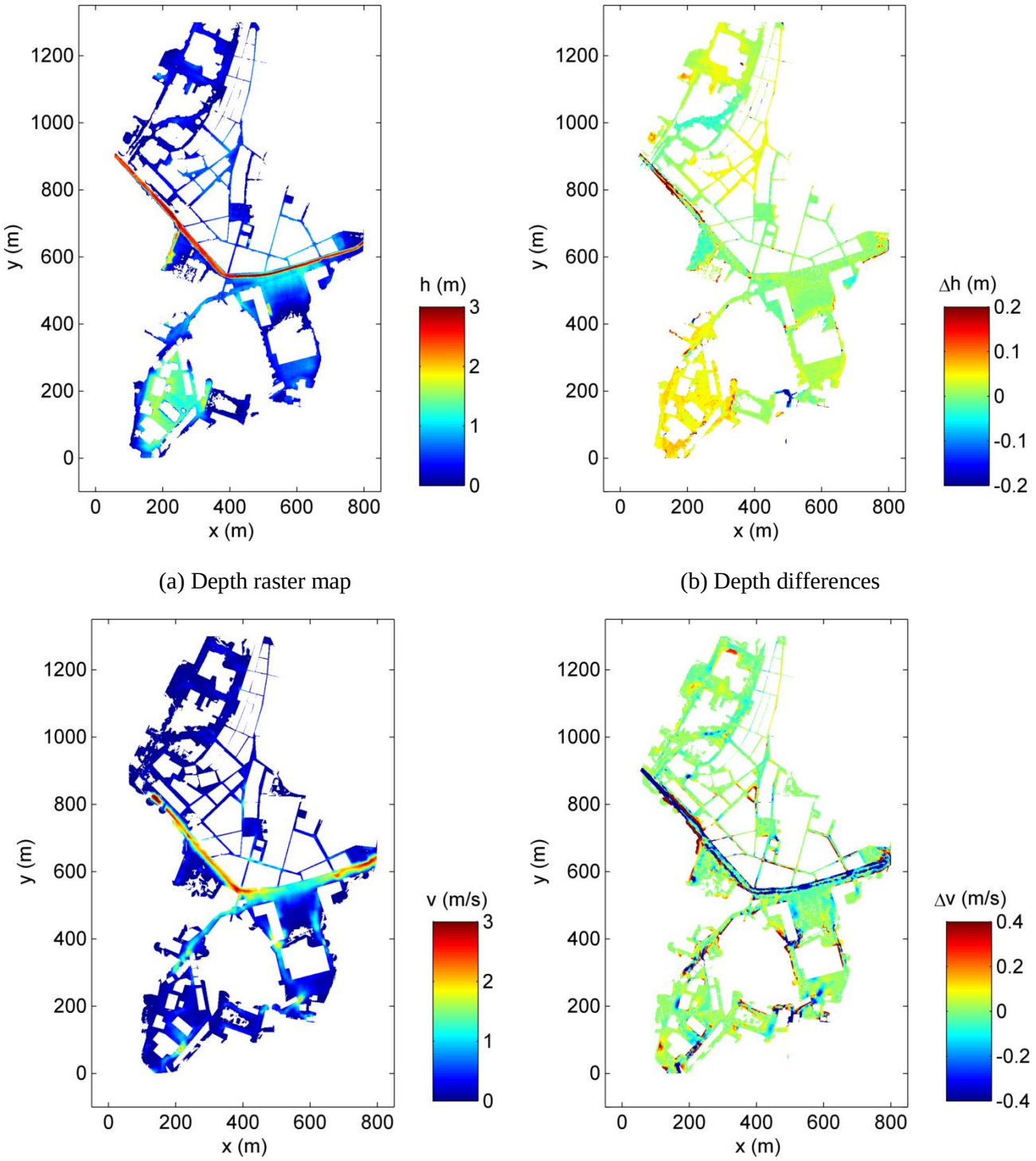

(a) Depth raster map

(b) Depth differences

(c) Velocity raster map

(d) Velocity differences

Figure 13. Example of depth and velocity raster maps based on the LS-SVM predictions (left) and depth and velocity differences with respect to the corresponding 2D-SWE map (right).

4. CONCLUSIONS

This paper presents the application of a non-parametric regression model based on least squares support vector machines for the spatial prediction of flood hazard. The model is tested in a coastal urban area, using the discharge in three main streams and the tidal level as the predictor variables to compute the spatial distribution of the maximum water depth and velocity in the urban area. The regression model shows a good performance in predicting maximum depths and velocities throughout the studied area, with mean absolute errors of 0.018 m in depth and 0.020 m/s in velocity. The model captures different non-linear relationships between the predictor and dependent variables, as reflected in the shapes of the rating curves at different control points. This good performance is independent of the range of depths and velocities achieved at the control points.

The model performs reasonably well for flood hazard mapping, especially if the degree of flood hazard is based only on flood depth (F1 score of 0.88). Due to its simplicity, reduced computation times and good performance, this approach offers great potential for applications such as real time forecasting or uncertainty propagation in a Monte Carlo context, using a 2D-SWE model as the basis to calibrate the LS-SVM model.

ACKNOWLEDGEMENTS

This work was financially supported by the Spanish Ministry of Economy and Competitiveness (Ministerio de Economía y Competitividad) within the project "CAPRI: Probabilistic flood prediction with high resolution hydrologic models from radar rainfall estimates" (reference CGL2013-46245-R). María Bermúdez gratefully acknowledges financial support from the Spanish Regional Government of Galicia, Plan I2C (Postdoctoral grant reference ED481B 2014/156-0).

The authors declare no conflict of interest.

REFERENCES

Apel, H. et al., 2009. Flood risk analyses—how detailed do we need to be? *Natural Hazards*, 49(1), pp.79–98.

Aronica, G., Bates, P.D. & Horritt, M.S., 2002. Assessing the uncertainty in distributed model predictions using observed binary pattern information within GLUE. *Hydrological Processes*, 16(10), pp.2001–2016.

Bermúdez, M. et al., 2018. Development and Comparison of Two Fast Surrogate Models for Urban Pluvial Flood Simulations. *Water Resources Management*, 32(8), pp.2801–2815.

Bermúdez, M. et al., 2017. Quantifying local rainfall dynamics and uncertain boundary conditions into a nested regional-local flood modeling system. *Water Resources Research*, 53(4), pp.2770–2785.

Bermúdez, M. & Zischg, A.P., 2018. Sensitivity of flood loss estimates to building representation and flow depth attribution methods in micro-scale flood modelling. *Natural Hazards*, 92(3), pp.1633–1648.

Bladé, E. et al., 2014. Iber: herramienta de simulación numérica del flujo en ríos. *Revista Internacional de Métodos Numéricos para Cálculo y Diseño en Ingeniería*, 30(1), pp.1–10.

Brabanter, K. De, Suykens, J.A.K. & Moor, B. De, 2013. Nonparametric Regression via **StatLSSVM**. *Journal of Statistical Software*, 55(2), pp.1–21.

Bruwier, M. et al., 2017. Shallow-water models with anisotropic porosity and merging for flood modelling on Cartesian grids. *Journal of Hydrology*, 554, pp.693–709.

Cea, L. et al., 2016. Rapid flood inundation modelling in a coastal urban area using a surrogate model of the 2D shallow water equations. In *Proceedings of the 4th European Congress of the International Association of Hydroenvironment engineering and Research, IAHR 2016*. pp. 850–855.

Cea, L., Bermúdez, M. & Puertas, J., 2011. Uncertainty and sensitivity analysis of a depth-averaged water quality model for evaluation of Escherichia Coli concentration in shallow estuaries. *Environmental Modelling & Software*, 26(12), pp.1526–1539.

Cea, L. & Bladé, E., 2015. A simple and efficient unstructured finite volume scheme for solving the shallow water equations in overland flow applications. *Water Resources Research*, 51(7), pp.5464–5486.

Cea, L. & French, J.R., 2012. Bathymetric error estimation for the calibration and validation of estuarine hydrodynamic models. *Estuarine, Coastal and Shelf Science*, 100, pp.124–132.

Cea, L. & Vázquez-Cendón, M.E., 2009. Unstructured finite volume discretization of two-dimensional depth-

averaged shallow water equations with porosity. *International Journal for Numerical Methods in Fluids*, 63(8), p.n/a-n/a.
Chang, L.-C. et al., 2010. Clustering-based hybrid inundation model for forecasting flood inundation depths. *Journal of Hydrology*, 385(1–4), pp.257–268.
Chen, A.S. et al., 2012. A coarse-grid approach to representing building blockage effects in 2D urban flood modelling. *Journal of Hydrology*, pp.1–16.
Comer, J. et al., 2017. Development of high-resolution multi-scale modelling system for simulation of coastal-fluvial urban flooding. *Natural Hazards and Earth System Sciences*, 17(2), pp.205–224.
Fraga, I. et al., 2016. Global Sensitivity and GLUE-Based Uncertainty Analysis of a 2D-1D Dual Urban Drainage Model. *Journal of Hydrologic Engineering*, 21(5), p.04016004.
Ghimire, B. et al., 2013. Formulation of a fast 2D urban pluvial flood model using a cellular automata approach. *Journal of Hydroinformatics*, 15(3), p.676.
Guidolin, M. et al., 2016. A weighted cellular automata 2D inundation model for rapid flood analysis. *Environmental Modelling & Software*, 84, pp.378–394.
Guinot, V., 2012. Multiple porosity shallow water models for macroscopic modelling of urban floods. *Advances in Water Resources*, 37, pp.40–72.
Horritt, M.. & Bates, P.D., 2002. Evaluation of 1D and 2D numerical models for predicting river flood inundation. *Journal of Hydrology*, 268(1–4), pp.87–99.
Jhong, B.-C., Wang, J.-H. & Lin, G.-F., 2017. An integrated two-stage support vector machine approach to forecast inundation maps during typhoons. *Journal of Hydrology*, 547, pp.236–252.
Kennard, R.W. & Stone, L.A., 1969. Computer Aided Design of Experiments. *Technometrics*, 11(1), p.137.
Kreibich, H. et al., 2009. Is flow velocity a significant parameter in flood damage modelling? *Nat. Hazards Earth Syst. Sci*, 9, pp.1679–1692.
Kroll, S. et al., 2017. Semi-automated buildup and calibration of conceptual sewer models. *Environmental Modelling and Software*, 93, pp.344–355.
Lin, G.-F., Lin, H.-Y. & Chou, Y.-C., 2013. Development of a real-time regional-inundation forecasting model for the inundation warning system. *Journal of Hydroinformatics*, 15(4), pp.1391–1407.
Liu, L. et al., 2015. Developing an effective 2-D urban flood inundation model for city emergency management based on cellular automata. *Natural Hazards and Earth System Science*, 15(3), pp.381–391.
Liu, Y. & Pender, G., 2015. A flood inundation modelling using v-support vector machine regression model. *Engineering Applications of Artificial Intelligence*, 46, pp.223–231.
Neal, J. et al., 2012. How much physical complexity is needed to model flood inundation? *Hydrological Processes*, 26(15), pp.2264–2282.
Pappenberger, F. et al., 2007. Fuzzy set approach to calibrating distributed flood inundation models using remote sensing observations. *Hydrology and Earth System Sciences*, 11(2), pp.739–752.
Polinsky, A. et al., 1996. Librain: software for automated design of exploratory and targeted combinatorial libraries. In I. . Chaiken & K. D. Janda, eds. *Molecular Diversity and Combinatorial Chemistry: Libraries and Drug Discovery, American Chemical Society, Washington, D.C.* pp. 219–232.
Razavi, S., Tolson, B.A. & Burn, D.H., 2012. Review of surrogate modeling in water resources. *Water Resources Research*, 48(7), p.W07401.
Schubert, J.E. & Sanders, B.F., 2012. Building treatments for urban flood inundation models and implications for predictive skill and modeling efficiency. *Advances in Water Resources*, 41, pp.49–64.
Solomatine, D.P. & Ostfeld, A., 2008. Data-driven modelling: some past experiences and new approaches. *Journal of Hydroinformatics*, 10(1), pp.3–22.
Stephens, E., Schumann, G. & Bates, P., 2014. Problems with binary pattern measures for flood model evaluation. *Hydrological Processes*, 28(18), pp.4928–4937.
Suykens, J.A.K. et al., 2002. *Least Squares Support Vector Machines*, World Scientific.
Tayefi, V. et al., 2007. A comparison of one- and two-dimensional approaches to modelling flood inundation over complex upland floodplains. *Hydrological Processes*, 21(23), pp.3190–3202.
Tsakiris, G., 2014. Flood risk assessment: concepts, modelling, applications. *Nat. Hazards Earth Syst. Sci*, 14, pp.1361–1369.
Vapnik, V.N., 1998. *Statistical learning theory*, Wiley.
Willett, P., 1996. Molecular diversity techniques for chemical databases. *Information Reseach*, 2(3).
Yaseen, Z.M. et al., 2015. Artificial intelligence based models for stream-flow forecasting: 2000–2015. *Journal of Hydrology*, 530, pp.829–844.

Yu, D. & Lane, S.N., 2006. Urban fluvial flood modelling using a two-dimensional diffusion-wave treatment, part 1: mesh resolution effects. *Hydrological Processes,* 20(7), pp.1541–1565.

FIGURE CAPTIONS.

Figure 1. River cross section of the synthetic case study.

Figure 2. Example of water depth map predicted by the 2D-SWE in the synthetic case study. Location of control points (P1-P4).

Figure 3. Topography used in the 2D-SWE model overlaid onto an aerial image of the study area. The arrows represent the upstream boundary conditions, which correspond to the three main watercourses of the basin.

Figure 4. Example of inflow hydrographs prescribed at the upstream open boundaries of the 2D-SWE model. The location of the three open boundaries (Q1, Q2 and Q3) is indicated in Figure 3.

Figure 5. Scatter plots of water depths computed with the 2D-SWE and the LS-SVM models in validation, considering: (a) Regression model A applied to predict peak depths only; (b) Regression model A applied to predict 5-min resolution water depths; (c) Regression model B applied to predict 5-min resolution water depths. Note: MAE is the global mean absolute error on the 4 points and for the ensemble of validation runs.

Figure 6. Water depth time series at control points P1, P3 and P4 computed with the 2D-SWE model and with the LS-SVM models in two illustrative simulations: (a) Simulation 1, regression model A; (b) Simulation 1, regression model B; (c) Simulation 2, regression model A; (d) Simulation 2, regression model B.

Figure 7. Global mean absolute error of the depth predictions (left) and the velocity predictions (right) in calibration and validation as a function of the number of calibration runs (k).

Figure 8. Two-dimensional histogram of the LS-SVM predictions vs. 2D-SWE predictions for the water depth (left) and velocity (right) using 100x100 bins. The color bar shows the relative frequency in the histogram, being the sum of all frequencies in each x-direction bin equal to unity.

Figure 9. Histogram of mean absolute error of depth and velocity predictions at the different points.

Figure 10. Scatter map of the MAE at each point in validation. The size of each marker is proportional to the MAE at that point. The location of the points represented in Figures 7 and 8 is marked by a black square.

Figure 11. Depth predictions (h) at four representative points (control points P1-P4 in Figure 6) with the 2D-SWE model and the LS-SVM model, as a function of the normalized maximum discharge of the main water course (Q1*).

Figure 12. Velocity predictions (v) at four representative points (control points P1-P4 in Figure 6) with the 2D-SWE model and the LS-SVM model, as a function of the normalized maximum discharge of the main water course (Q1*).

Figure 13. Example of depth and velocity raster maps based on the LS-SVM predictions (left) and depth and velocity differences with respect to the corresponding 2D-SWE map (right).

TABLES

Table 1. Mean performance of the LS-SVM model based on the hazard mapping, considering all the validation runs: precision (p), recall (r) and F1 score.

	Flood extent	Flood hazard					
	h>0.10 m	h>0.20 m	h>0.50 m	h>1 m	v>0.10 m/s	v>0.50 m/s	v>1 m/s
p	0.84	0.89	0.88	0.87	0.70	0.73	0.78
r	0.94	0.92	0.93	0.93	0.88	0.79	0.69
F1	0.87	0.89	0.88	0.88	0.76	0.75	0.72